

Design and Fabrication of Silicon Nanowire based Sensor

Siti Fatimah Abd Rahman¹, Nor Azah Yusof^{1,3,}, Uda Hashim², M. Nuzaihan Md Nor²*

¹Institute of Advanced Technology, Universiti Putra Malaysia, 43400 UPM Serdang, Selangor, Malaysia

²Institute of Nano Electronic Engineering, Universiti Malaysia Perlis, 01000 Kangar, Perlis, Malaysia

³Chemistry Department, Faculty of Science, Universiti Putra Malaysia, 43400 UPM Serdang, Selangor, Malaysia

*E-mail: azahy@upm.edu.my

This paper reports the process development of silicon nanowires sensor requires both the fabrication of nanoscale diameter wires and standard integration to CMOS process. By using silicon-on-insulator (SOI) wafer as a starting material, the nanowires is fabricated using a top-down approach which involved Scanning Electron Microscope based Electron Beam Lithography method. The silicon nanowires are well developed with the smallest dimension is 65nm in width. The effect of line width and exposure dose on the pattern structure is investigated experimentally using the negative photoresist ma-N2403 for EBL. The exposure doses for the resist layer are varied in the range of 50 μ C/cm² to 180 μ C/cm² at 20 kV accelerating voltage with a beam current of 0.075nA. The nanowires resist masks are well developed with dimension less than 100 nm in width for the dose exposure parameters of 80 μ C/cm², 100 μ C/cm² and 120 μ C/cm². Subsequently, the two metal electrodes which are designated as source and drain are fabricated on top of individual nanowire using conventional lithography process. Morphological, electrical and chemical characteristics have been proposed to verify the outcome of the fabricated device. Finally, the fabricated device is performed as pH level detection. Three types of standard aqueous pH buffer buffer solutions which are pH 4, pH 7 and pH 10 are used to test the electrical response of the device. The SiNWs sensor show the highest resistance value for pH 4 and the lowest resistance value for pH 10. In terms of sensitivity, the device with smaller nanowire is found to be more sensitive than larger nanowire as a result of the high surface-to-volume ratio.

Keywords: electron beam lithography, silicon nanowire, resistivity, ph detection

1. INTRODUCTION

The creation of minuscule size sensors is the main application of nanotechnology. Low cost materials, reduced weight, easily integrated to the existing system and required lower power

consumption are the significant advantages in the reducing sensor size [1]. This advantageous has motivated many researchers to develop nanostructures to be as a suitable base for sensing element as well as maintaining the historical trend of scaling down the electronic devices [2]. Among the nanostructures, nanowires (NWs) emerge as one of the best defined and controlled classes of the nanoscale building blocks in biosensing. These materials are attractive because they have very narrow diameters and provide a link between molecular and solid state physics [2,3]. Due to quantum confinement effects and their high surface area-to-volume ratios, NWs can be proposed as chemical and biological sensing element [4].

The basic idea for using NWs for sensing is to measure its conductance which is affected by the charges on its surface. Binding with the surface of these NWs, alters their ability to conduct which serves as the detection mechanism [5]. The schematic in Fig. 1 (a) shows the principle of the nanowire sensor where the current is changed, $I \rightarrow I + \Delta I$, due to the attached charges molecules [6]. In such sensing devices, the two metal electrodes which are designated as source (S) and drain (D) of a device is bridged by nanowires. Binding to the surface of these nanowires alters their ability to conduct, which serves as the detection mechanism. Fig. 1 (b) provides illustration of a silicon nanowire as a sensing device.

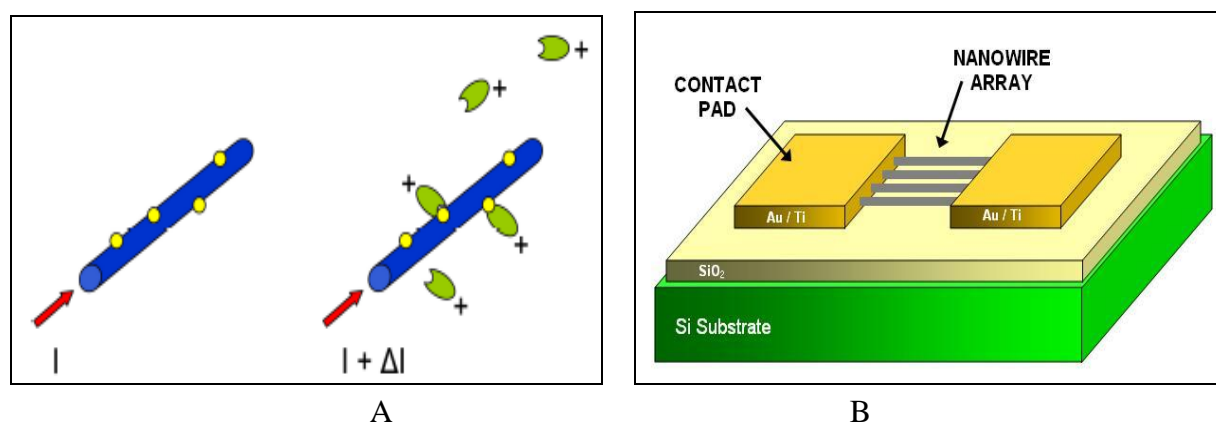


Figure 1. (a) Schematic showing the principle of the NW sensor. The surface is coated with receptor molecules (yellow). As charged molecules (green) attaches to the receptor molecules the current is changed [6]. (b) Schematic of a fabricated device showing metal source and drain electrodes with the nanowire as the bridge.

However, existing SiNW sensor have had some technical problems such as poor controllability of electrical properties and difficulty of integration to other existing microelectronic components [7]. This is due to bottom-up synthesized SiNW which have large statistical variation in the electrical properties and difficult to manipulate for the reliable integration to other microelectronic component [8]. In addition, good ohmic contact between the synthesized SiNW with metal interconnection is difficult to achieve. Besides, there is also a weak point of the synthesized SiNW which is the incompatibility with CMOS process. SiNW grown via metal-catalyzed chemical vapor deposition (CVD) process contain of metal elements such as gold or copper. Therefore integration of these SiNW is not compatible to the CMOS process [8,9]. For this reason, this work demonstrates the top-down

approach for device fabrication to create SiNW biosensor which shows significant advantages in small size and low cost. The top-down nanofabrication method by electron beam lithography (EBL) and integrated with CMOS process such as reactive ion etching (RIE) is implemented for device structure formation.

2. EXPERIMENTAL

2.1 Mask design

The creation of the NW design is done beforehand using a computer aided design (CAD) program developed by Raith GmbH, named ELPHY Quantum. ELPHY Quantum is a universal lithography system which makes it possible to produce micro and nano structures by means of electron beam writing in connection with scanning electron microscope (SEM) system. The operating software of ELPHY Quantum is known as Quantum GDS II Editor. The layout design of the NW using Quantum GDS II is shown in Fig. 2. In creating these mask layout, certain design constraints were taken into consideration. A long NW with dimension of $400\ \mu\text{m}$ is designed to assure the NW to be in contact with the electrode pad in the forthcoming fabrication process. In addition, arrays of NWs are designed to increase the probability of adhesion or reaction of the analytes to the nanowire surface during the testing part. The NWs arrays are separated by $40\ \mu\text{m}$ gaps to allow for future capability of the development and etching process.

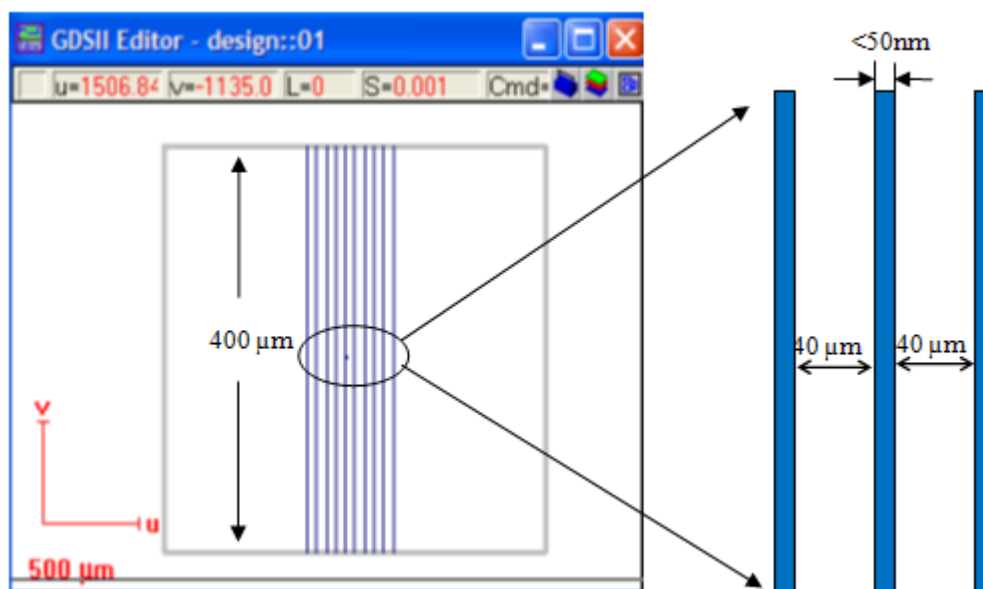


Figure 2. (a) nanowire designed by using Elphy Quantum GDS II with dimension of the design

Conventional photolithography is utilized to fabricate the millimeter size of structures namely alignment marks, electrode pads and test channels. This technique is used to transfer the designed

pattern from the mask onto the sample surface and is carried out using MIDAS MDA-400M Mask Aligner. Masks are used as a stencil to generate patterns onto a resist coated wafer. The mask contains black and transparent areas that respectively hinder or allow ultraviolet rays penetrate through. The designs are made with the aid of the drawing software, AutoCAD. A total of three designs namely alignment mark, electrode pad and test channel are designed in order to create a complete SiNWs sensor device.

2.2 Top-down device fabrication

The 4-inch (100 mm in diameter) p-type silicon on insulator (SOI) wafer which initially had a 160 nm silicon layer on a 200nm buffered-oxide (BOX) insulating layer with resistivity 1-20 Ωcm was used as the starting material in this work. Standard cleaning procedure using RCA1, BOE, and RCA 2 was introduced to remove organic and inorganic contaminant on the samples' surface followed by washing in de-ionized water for the last steps. Then, the samples were dried on a conduction hot plate at 200°C for 5 minutes to remove residual water and cooled down in room temperature for 10 minutes.

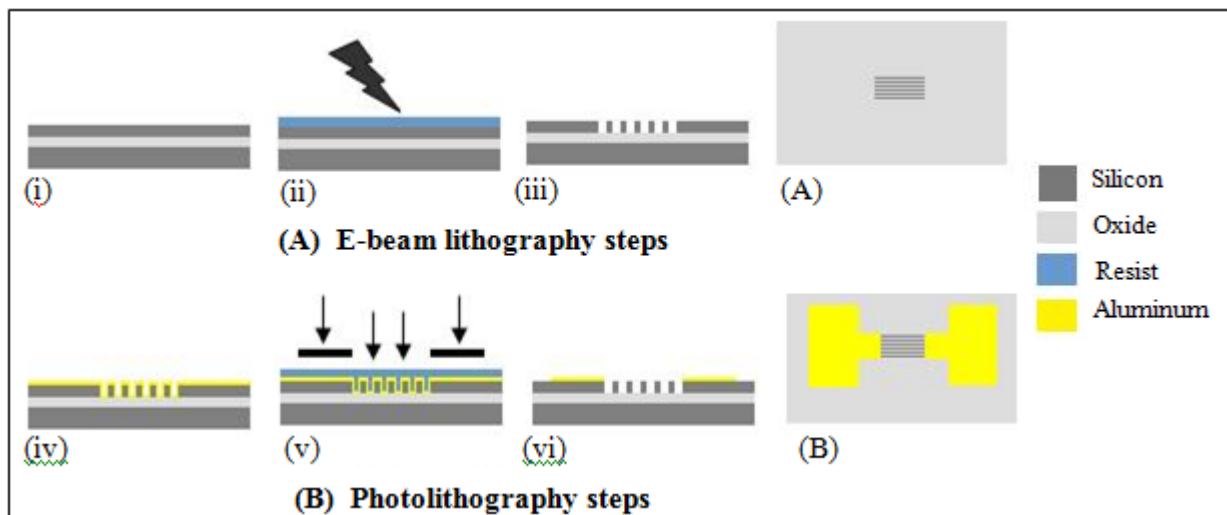


Figure 3. Experimental scheme of electron beam lithography coupled with optical lithography. (i) a cleaned SOI sample (ii) coated sample is exposed using EBL (iii) after development process and resist strip (A) top view of SiNWs fabricated using EBL (iv) electron beam evaporation of Au onto the sample surface (v) optical lithography exposure (vi) wet etching of a deposited Au layer using the resist as mask (B) top view of aligned SiNWs source and drain pad.

Fig. 3 illustrates the general steps of EBL and optical lithography which are implemented in this work. The process started with EBL process to fabricate nanowire as shown in Figure 2 part A. The negative tone photoresist of ma-N 2403 was spin coated at 3000 rpm, and pre-baked on the hot plate at 90° C for 90 seconds. The resist coated samples were exposed to a nanowire pattern using 20 keV electrons and beam current of 0.075 nA. The electron dose was varied in the range of 80 -180 $\mu\text{C}/\text{cm}^2$. The exposed samples were developed in the metal free developer ma-D 525, and then post

baked on the hotplate at 90° C for 90 seconds. Reactive ion etching (RIE) process was utilized to fabricate Silicon nanowire using the nanoscale pattern resist as the etching mask. Then, Al layer was deposited on the sample surface using physical vapor deposition (PVD) and followed by optical lithography to pattern deposited Al electrodes contacting both ends of the fabricated nanowires as illustrated in Fig. 3 part B. Next, the electrical measurements were done using a Keithley semiconductor parametric analyzer (SPA). Dry testing of the fabricated nanowires was performed to measure the current-voltage (I-V) properties of the device. In order to demonstrate the usefulness of the fabricated sample as a sensing device, the unmodified SiNW sensor device is then used for the pH measurements.

3. RESULTS AND DISCUSSION

3.1. Optimization of nanowire resist mask

The resist mask formation is the important step in this research work. Considering the dry etching process for the next step, the resist mask should be developed according to the design width so as to obtain patterns which have a high aspect ratio. For the exposure process, many contributing parameters such as beam current, write field size, area step size, dwell time, area dose and exposure time are considered in order to complete this process.

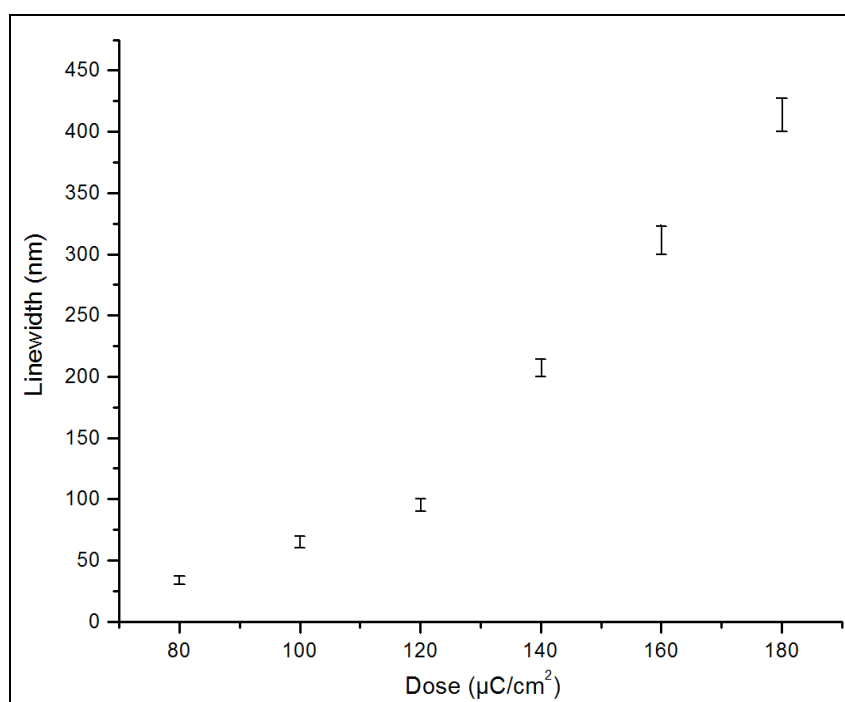


Figure 4. Developed resist linewidth for various electron doses of 80-180 $\mu\text{C}/\text{cm}^2$.

The acceleration voltage applied to the beam determines the intensity of the beam current [10]. In order to determine the current, the measurement is performed by focusing the beam with 20 kV of acc voltages on a Faraday cup. During the beam focusing, the spot size is adjusted until a stable beam current of 0.075 nA is achieved. Smaller spot size is required in order to get the smaller beam. Thus, the range of the spot size used in this work is controlled between 40 – 45. As the beam increases, the larger the beam width grows and will affect the dimension results of the fabricated structures [11]. Also, line edge roughness or pattern distortion is observed on the exposed pattern. This is due to the effect of electron scattering in resist and substrate, known as the proximity effect [12]. The net result of the electron scattering is that the dose delivered by the electron beam tool is not confined to the shapes that the tool writes, resulting in pattern specific line width variations [13]. One of the strategies to minimize the proximity effect is doses variation. By keeping the same design (50nm) for every exposure with different value of doses (80-180 $\mu\text{C}/\text{cm}^2$), the corresponding results are shown in Fig. 4.

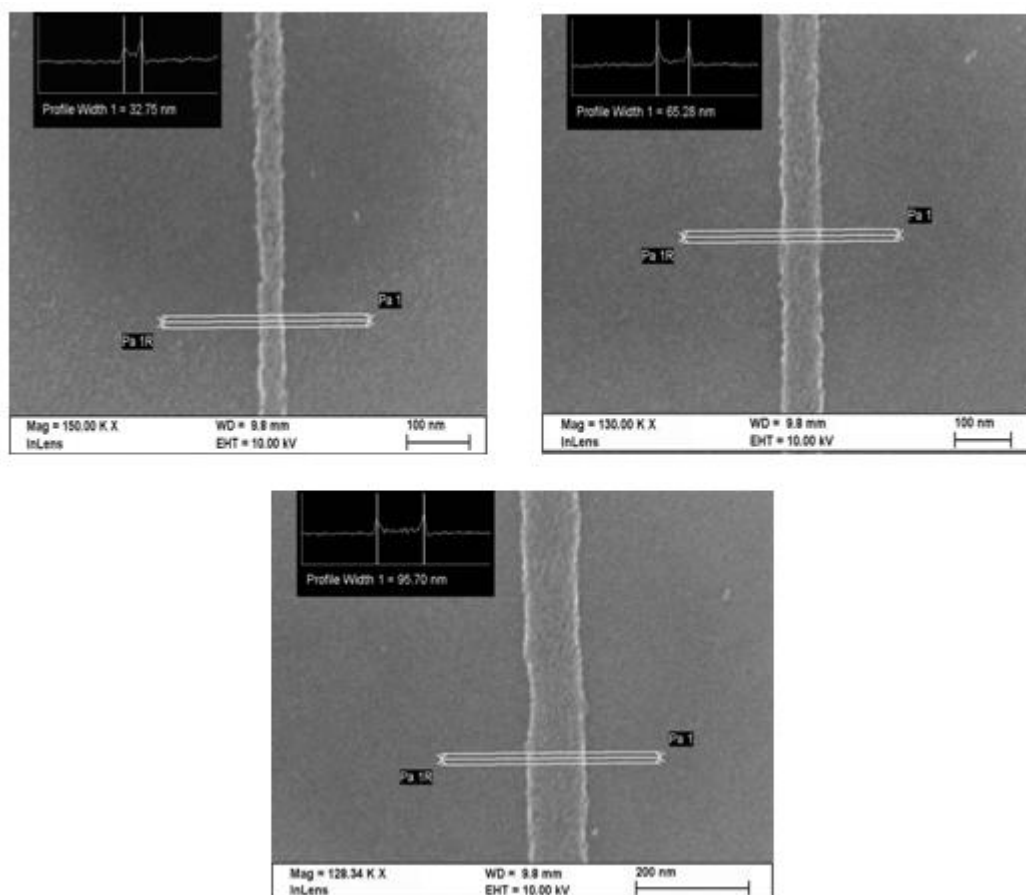


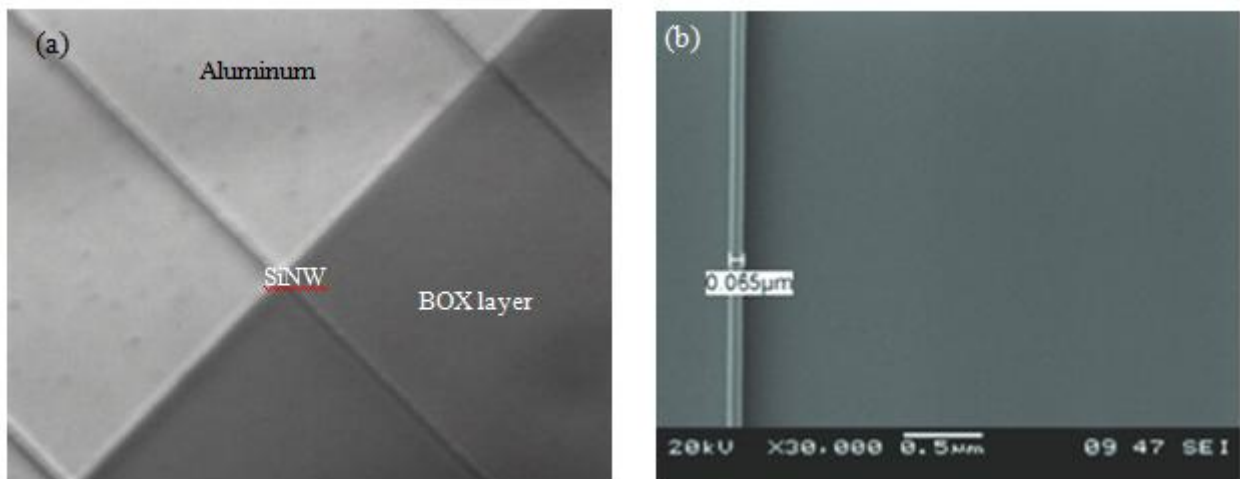
Figure 5. The SEM images of the developed resist mask for the wire diameter less than 100nm obtained at doses in the range of $80\mu\text{C}/\text{cm}^2$ to $120\mu\text{C}/\text{cm}^2$.

As the first step for nanowire development the effects of the design width and dose are controlled to get the narrow line of the wires down to 100nm in size. The experiments have shown that, the pattern structure is affected by the dose. By increasing the dose, the line width would also be

increased. The target size of nanowire resist mask less than 100nm was accomplished by employing the exposure doses of $80\mu\text{C}/\text{cm}^2$, $100\mu\text{C}/\text{cm}^2$ and $120\mu\text{C}/\text{cm}^2$. Based on the 50nm actual design specification with the mentioned exposure parameters, the average of NW mask with the dimensions of approximately 33nm, 66nm and 96nm is achieved (Fig. 5). In addition, by increasing the value of the dose to $140\mu\text{C}/\text{cm}^2$, $160\mu\text{C}/\text{cm}^2$ and $180\mu\text{C}/\text{cm}^2$, the developed resist mask is turned to micro dimension which is in average of approximately $0.2\mu\text{m}$, $0.3\mu\text{m}$ and $0.4\mu\text{m}$. It is shown that, when the exposure dose is exceeded from the required value, the line pattern becomes uncontrolled. This is due to the proximity and accumulation effects of e-beam lithography [14]. Besides, by increasing the electron beam dose, the line widths generally become wider due to the impact of the dose applied on pattern. As the dose increases, more electrons are transferred on the same design area and the line-widths become thicker. The thicker line widths have been translated in the form of an increase in width or length of the pattern design with the increment of doses [15,16].

3.2 Morphological and Physical Characterizations

In this electron beam coupled with conventional lithography process, the source and drain pads are well aligned on top of the fabricated nanowires to make a reliable contact between the metal pads and the semiconductor nanowires. The fabricated structures are characterized using the SEM image and 3D nanop profiler. Fig. 6 (a) shows the close-up view of the SiNW underlying the Al contact pad. The SiNWs structures form as islands on oxide (BOX) layer and Fig. 6 (b) shows the SEM image of the 65nm SiNW. This close-up view image is then converted into a 3D image to perform its measurement value as depicted in Fig. 6 (c). For NWs structures, the image and color are not obviously appeared. Possibly this is due to the thickness of the SiNW structures which are too thin. However, when the data analysis has been done, it shows the ideal result for the SiNW profile. Based on the result, NW with a diameter of 65nm and height of approximately 160nm is achieved. It clearly shows that, the SiNW is not well vertically etched. The top width of the SiNW is smaller than its base width. This possibility is due to the NW resist mask formation.



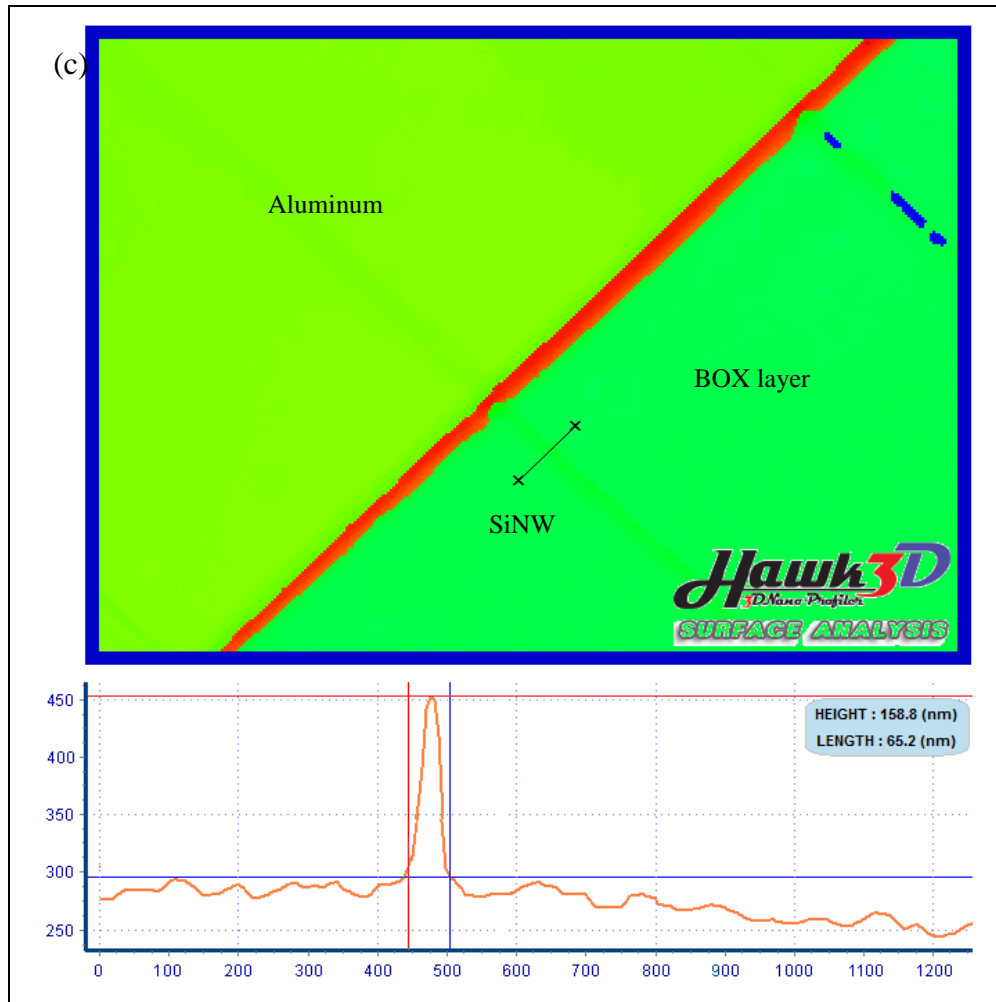


Figure 6. The images of (a) overall pattern structure fabricated on the sample (b) zoom in of the fabricated nanowire under Al pad layer and (c) 65nm of SiNW profile.

The resist profile depends on dose and development process. Increasing the dose value as well as development time will increase the undercut angle of the resist profile. The undercut occurs when the resist's base width is larger than its top width.

3.3. Electrical Characterization

Once the SiNWs has been formed as a two-terminal sensing device, its current-voltage (I-V) characteristic is then measured by using a Keithley 4200 Semiconductor Parameter Analyzer. During the measurement set-up, a typical resistor setting is employed on to the two terminal NW devices by supplying voltages to the source (S) region and obtains the output current at the drain (D) region as shown schematically in Fig. 7. For this experimental, devices with different width (W) of wires approximately (W = 65nm, 100nm, 200nm, 300nm and 400nm) were characterized. The purpose was to analyze the size dependence of wires to the device's electrical properties.

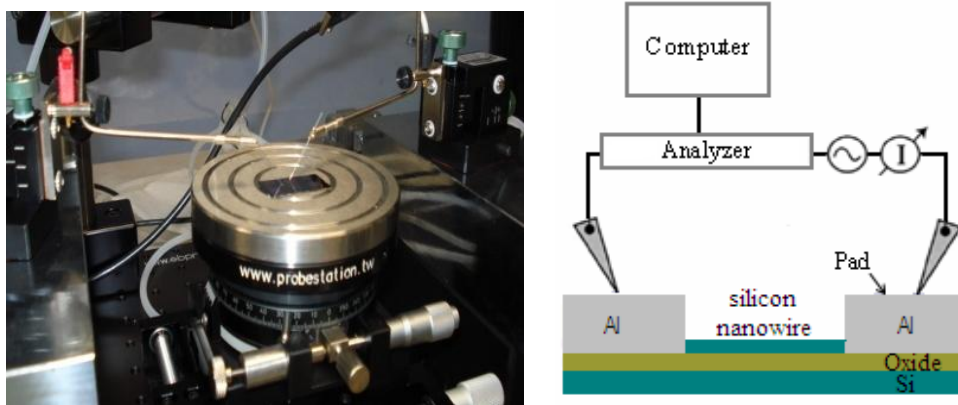


Figure 7. Schematic of the measurement circuit.

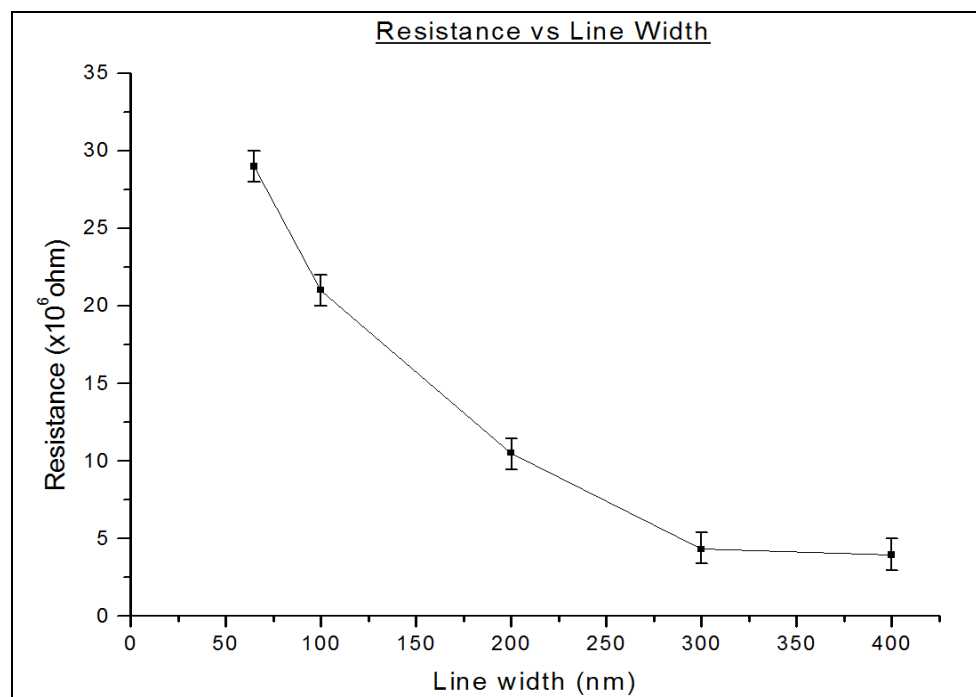


Figure 8. Electrical resistance of devices dependent on the width of wire.

As shown by the data points in Fig. 8, indicating that the device's resistivity values are related to the width of the Si wire. The average resistance of the fabricate devices with the wire width approximately of 65 nm, 100 nm, 200 nm, 300 nm and 400 nm were 29.11 M Ω , 20.01 M Ω , 9.46 M Ω , 3.43 M Ω and 2.981 M Ω , respectively. It is shown that, the resistance of the wire is inversely proportional to its width. As the wire gets smaller in dimension, the electrical resistance becomes higher. This is due to the increased surface-area-to-volume ratio for smaller dimensions of NW which has resulted greater surface effects on the electrical conduction [17]. The surface contamination effects of SiNWs such as surface damage, defects and trapped charges developed through the plasma etching process give significant roles for smaller NW due to the larger surface-to-volume ratio [17,18]. Thus, it has been shown that the electrical characterization of the devices depends strongly on the width of the

wires; resistance value increases with the decreasing NW width due to the surface-to-volume ratio effect.

In order to improve the device's performance, the samples were then employed for the thermal annealing process. Thermal annealing is accomplished by using rapid thermal annealing (RTA) system because of its effectiveness in terms of time and temperature compared to the conventional annealing using furnace. The device was annealed in pure nitrogen (N_2) gas at 300°C for 15seconds. Once the annealing process is performed, the resistance values of annealed devices are measured and compared as shown in Fig. 9 and Table 1 respectively.

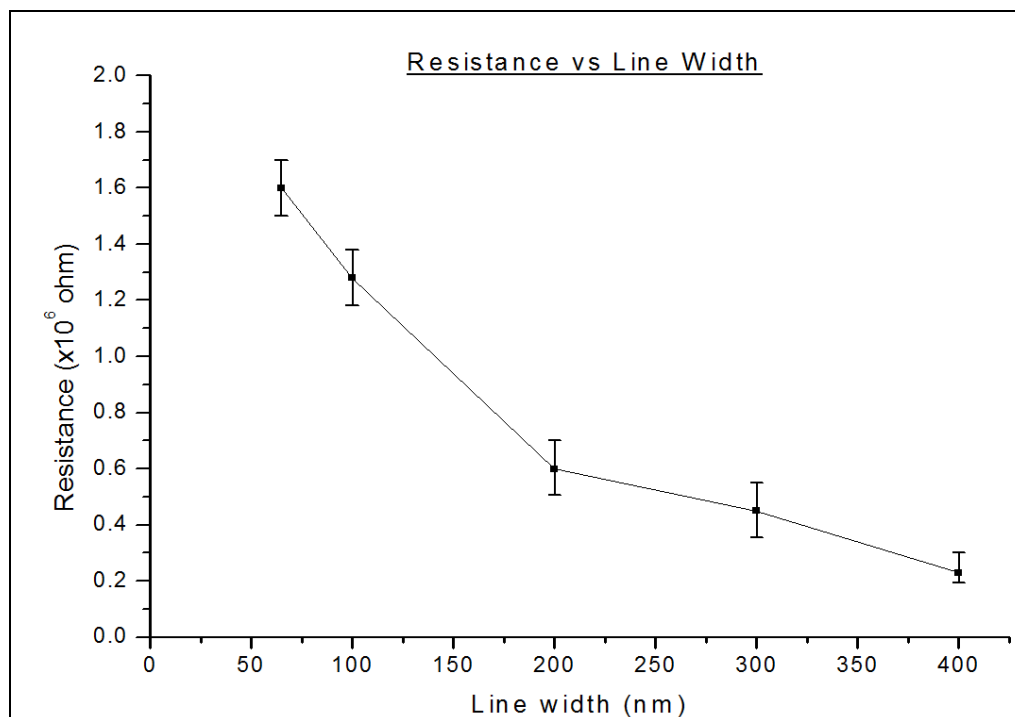


Figure 9. Electrical resistance of devices after thermal annealing process.

Table 1. Effect of thermal annealing on the resistance of the devices.

| Line width (nm) | Average resistance ($M\Omega$) | |
|-----------------|----------------------------------|-----------------|
| | Before annealing | After annealing |
| 65 | 29.11 | 1.60 |
| 100 | 20.01 | 1.28 |
| 200 | 9.46 | 0.60 |
| 300 | 3.43 | 0.45 |
| 400 | 2.98 | 0.19 |

Significant improvement in ohmic characteristics is observed in the annealed devices as shown in Fig. 9. The devices showed a high contact resistance before performed thermal annealing process, which is due to the poor contacts between the Al electrodes and the SiNW [2]. As a result, thermal

annealing process is introduced to facilitate a good ohmic contact between Al and Si [2,17]. This is probably due to the formation of aluminum silicide (Al_4Si_3) between the metal electrodes and the SiNW, which leads to a decrease in the contact resistance [2]. The devices with smallest line width of wires which is 65nm and 100nm shows the greatly improved of electrical resistance compared to the wider wires (microwires). According to Kar (2009) [19], this is due to the high surface-area-to-volume ratio as the wires getting smaller. This mean, the greater the surface for the same volume, the greater the surface effects (reactivity). Thus, the devices with the smaller wires (nanowires) exhibit large resistance changes while larger wires only show a little change of resistance value. In addition, by employing the thermal annealing process, the surface defects and trapped charge generated during the fabrication process may also be reduced [20]. This shows that the device annealing is an alternative way to obtain reliable electrical transport measurement results.

3.4 pH Level Detection

In order to prove the effectiveness of the fabricated SiNW device as a sensing tool, a chemically test has been done by demonstrating the device for the case of pH sensing. For this purpose, commercially available pH buffer solutions which are pH 4, pH 7 and pH 10 from QREC were used in this research work. For experimental set-up, the device was first connected to the SPA system. A constant volume (0.6 to 1.00 μL) of pH buffer solutions controlled by the syringe pump was carefully dropped onto the SiNWs surface assisted by microscope observation. To protect the solution from shortcutting the metal electrodes, three layers of positive resist were spun on the sample. The response of the device to the buffer solutions was recorded using a Keithley 4200 SPA based on a change of electrical signal measurement. A schematic of this experimental set-up is shown in Fig. 10.

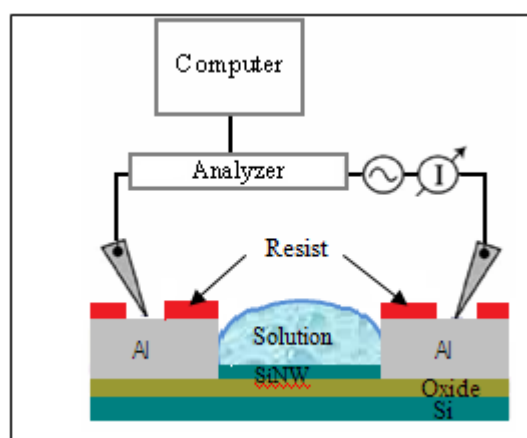


Figure 10. Schematic of the experimental setup. Solution is dropped onto the SiNW surface and red layer represent the resist passivation layer on top of Al electrodes.

Fig. 11 shows the measurement of resistance as a function of pH solution for two tested sample. The devices demonstrate the same behavior of curve trend which are pH 10 at the top,

followed by pH 7 and pH 4 at the bottom. These trends are in agreement with the previous research reported by Park et al. [21]. The resistance for sample A is higher at pH 4 which is $2.087\text{M}\Omega$, $1.939\text{M}\Omega$ at pH 7 and it becomes lowest to $1.781\text{M}\Omega$ at pH 10. Similar trend can be described to sample B which is the highest resistance is $1.587\text{M}\Omega$ at pH 4, $1.462\text{M}\Omega$ at pH 7 and the lowest is $1.347\text{M}\Omega$ at pH 10. It is showed that acid solution causes an increase in resistance while basic solution causes a decrease in resistance. Table 2 summarizes the average resistance for all pH tested samples.

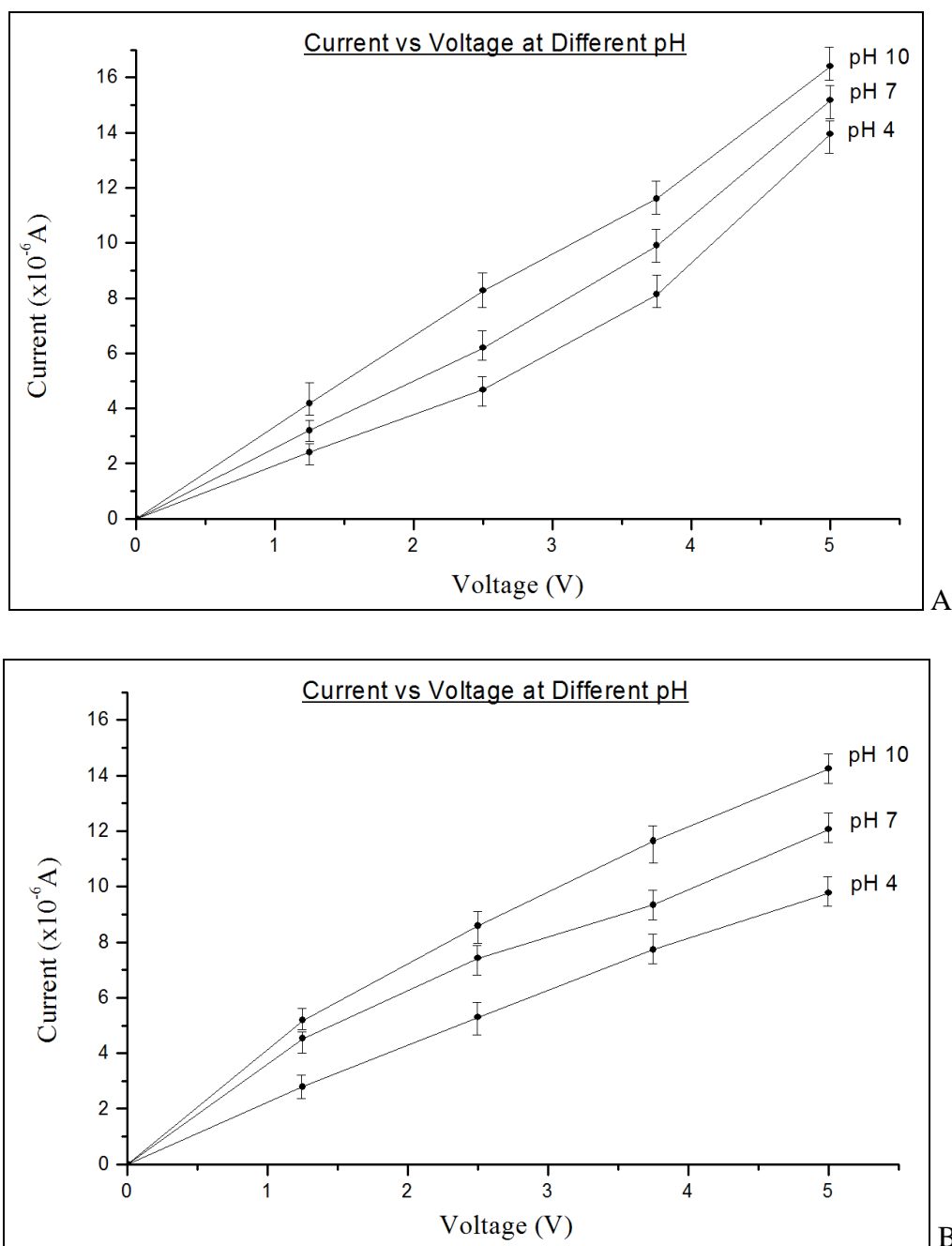


Figure 11. The device resistance responses to the pH change for (a) Sample A with SiNWs width approximately 65nm and (b) Sample B with SiNWs width approximately 100nm.

Table 2. Electrical responses of tested samples with different width of wires to the pH4, pH7 and pH10.

| Line width (nm) | Average resistance (MΩ) | | |
|-----------------|-------------------------|-------|-------|
| | pH 4 | pH 7 | pH 10 |
| 65 | 2.087 | 1.939 | 1.781 |
| 100 | 1.587 | 1.462 | 1.347 |
| 200 | 0.708 | 0.670 | 0.641 |
| 300 | 0.508 | 0.488 | 0.468 |
| 400 | 0.207 | 0.201 | 0.196 |

The pH response of SiNWs is determined by the interaction of the surface silanol (SiOH) group with the proton (H^+) ions. As reviewed, silanol groups (SiOH) can be found on an oxidized Si surface. These can be charged if buffer solution is added to the surface [6,21]. This phenomenon is experienced by the unmodified SiNWs device in reaction with the pH solution. As the H^+ ions are more in acidic solution (pH 4), the SiOH group is protonated to $SiOH_2^+$. More positive surface charge is developed and thus the SiNW surfaces become depleted of charge carriers (hole). As a result, the resistance for pH 4 increases. Conversely, for basic solution, the SiOH group become deprotonated to SiO^- . This process generates more negative ions on the NWs surface and thus less hole carrier depletion occurs. Consequently, the resistance for basic solution (pH 10) decreases. The reaction between SiOH groups of the SiO_2 and H^+ ion in solution is illustrated in Fig. 12.

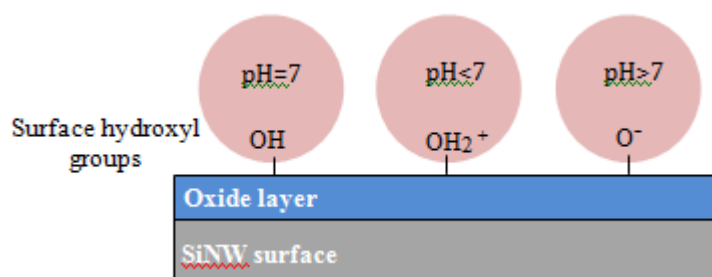


Figure 12. Schematic of the surface oxide. At low pH the hydroxyl groups is protonated (OH_2^+) while at high pH the hydroxyl groups get deprotonated (O^-).

Furthermore, in this work, the sensitivity of devices in terms of their wires size effects also investigated. Samples with different sizes of NWs which is 65nm, 100nm, 200nm, 300nm and 400nm are used to test their sensitivity to the pH level change. When immersed in an acidic buffer solution (pH 4), smaller NW exhibit large resistance changes while larger wires only show a little change of resistance value as shown in Fig. 13. The sensitivity (S) of the SiNW sensor can be defined as the relative change in resistance and can be expressed as $S = \Delta R / R_0$, where R_0 is the initial resistance and ΔR is the change in resistance [22]. By using this equation, the S values for the tested devices are tabulated in Table 3.

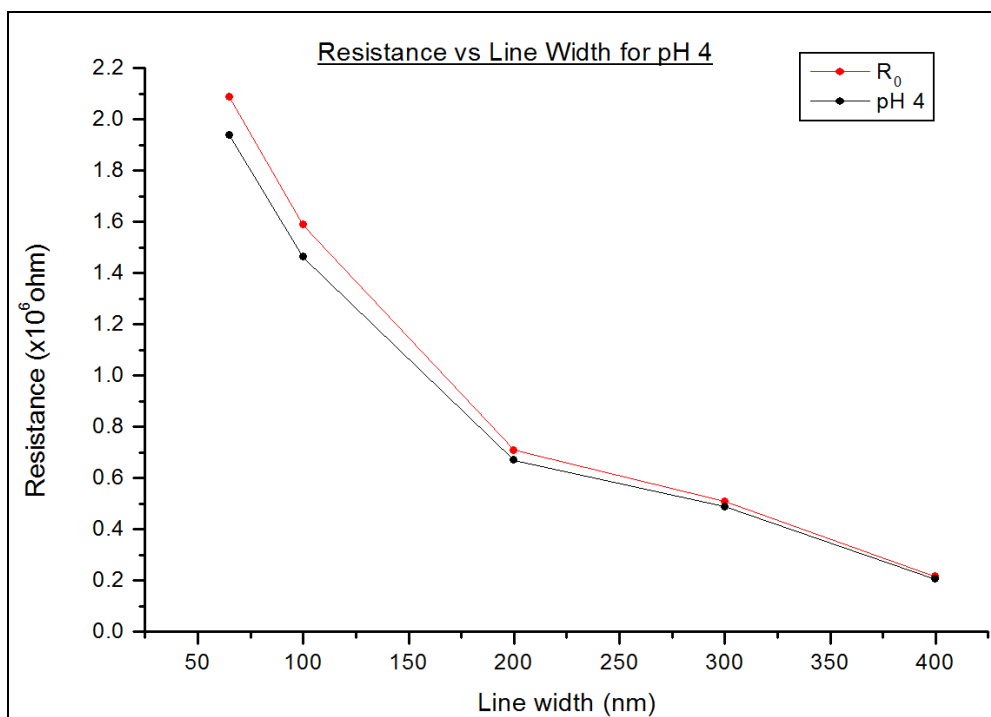


Figure 13. The average resistance of SiNWs ($W = 65\text{nm}$, 100nm , 200nm , 300nm and 400nm) samples before and after tested for pH4.

Table 3. Size dependence of the sensitivity to the width of SiNWs.

| Line width (nm) | Average resistance (M Ω) | | S= $\Delta R/R_0$ (%) |
|-----------------|----------------------------------|------------|-----------------------|
| | R_0 | ΔR | |
| 65 | 1.600 | 0.487 | 30 |
| 100 | 1.280 | 0.307 | 24 |
| 200 | 0.600 | 0.108 | 18 |
| 300 | 0.450 | 0.058 | 13 |
| 400 | 0.190 | 0.017 | 8 |

The results show that the sensitivity (S) increases with smaller diameter of wires. This behavior is ascribed to the larger surface-to-volume ratio and the small cross-section available for conduction channel for smaller wires. In short, the sensitivity of the device is dependent upon their size width which a smaller NW shows higher sensitivity by the high surface-to-volume ratio [15].

4. CONCLUSION

In this electron beam coupled with conventional lithography process, the source and drain pads are well aligned on top of the fabricated NWs to make a reliable contact between the metal pads and the semiconductor NWs. The fabricated device is then characterized using SPA in terms of current-voltage (I-V) relations. The comparison among the devices with different SiNW width demonstrates

the resistance of the NW is inversely proportional to its width. Smaller NW exhibit high resistance due to the increase of the surface-area-to-volume ratio. It has been observed that the device's performance is greatly improved after employing the thermal annealing process. Better Al-Si ohmic contact is obtained and thus the sample shows a decreasing value of resistance. In terms of sensing functionality, the fabricated device has demonstrated the potential device in the pH level detection. It can be observed that as the pH level increases, the resistance value decreases.

ACKNOWLEDGEMENTS

The author would like to thank National Nanotechnology Directorate (NND), MOSTI for financially supported and the members of Microelectronic's Cleanroom, Universiti Malaysia Perlis (UniMAP) and Chemistry Lab (UPM) for technically and theoretically supported.

References

1. B. Bhushan, *Springer Handbook of Nanotechnology*, Springer Berlin Heidelberg New York (2006).
2. C. K. Frederick, K. W. Wong, Y. H. Tang and Y. F. Zhang, *Applied Physics Letters*, 75 (1999) 1700.
3. L. Gorton, *TrAC Trends in Analytical Chemistry*, 12 (1993) 37.
4. D. Wang, B. A. Sheriff, M. McAlpine and J. R. Heath, *Nano Research: Springer*, 1 (2008) 9.
5. D. Grieshaber, R. MacKenzie, J. Voros and E. Reimhult, *Sensors*, 8 (2008) 1400.
6. N. Elfstrom, *Silicon Nanowires for Biomolecule Detection*, Royal Institute of Technology, Sweden (2008).
7. X. Y. Zhang, L. D. Zhang, Y. Lei, L. X. Zhao and Y. Q. Mao, *Materials Chemistry*, 11 (2001) 1732.
8. Y. Cui, Z. Zhong, D. Wang, W. U. Wang and C. M. Lieber, *Nano Letters*, 3 (2003) 149.
9. Y. Civale, L. K. Nanver, P. Hadley, E. J. G. Goudena and H. Schellevis, *IEEE Electron Device Letter*, 27 (2006) 343.
10. G. Rius, A. Verdaguer, F. A. Chaves, I. Martin, P. Godignon, E. L. Tamayo, D. Jimenez and F. P. Murano, *Microelectronic Engineering*, 85 (2008) 1413.
11. C. Vieu, F. Carcenac, A. Pepin, Y. Chen, M. Mejias, A. Lebib, L. Manin-Ferlazzo, L. Couraud and H. Launois, *Applied Surface Science*, 164 (2000) 111.
12. J. Du, Z. Cui, X. Yuan and Y. Guo, *Microelectronic Engineering*, 61 (2002) 265.
13. M. A. McCord and M. J. Rooks, *Handbook of Microlithography, Micromachining and Microfabrication*, SPIE, Bellingham, Washington (1997).
14. H. Elsner, H. G. Meyer, A. Voigt and G. Grützner, *Microelectronic Engineering*, 46 (1999) 389.
15. H. Elsner and H. G. Meyer, *Microelectronic Engineering*, 5 (2001) 291.
16. S. F. Hu, W. C. Weng and Y. M. Wan, *Solid State Communications*, 130 (2004) 111.
17. I. Park, Z. Li, A. P. Pisano and R. S. Williams, *Biosensors and Bioelectronics*, 22 (2007) 2065.
18. J. D. Plummer, M. D. Deal and P. B. Griffin, *Silicon VLSI Technology Fundamentals, Practice and Modeling*, Prentice Hall, New Jersey, U.S.A (2000).
19. B. Yu, L. Wang, Y. Yuan, P. M. Asbeck and Y. Taur, *Electron Devices*, 55 (2008) 2846.
20. I. Park, Z. Li, A. P. Pisano and R. S. Williams, *Nanotechnology*, 21 (2010) 1.
21. A. Tarasov, M. Wipf, R. L. Stoop, K. Bedner, W. Fu, V. A. Guzenko, O. Knopfmacher, M. Calame and C. Schonenberger, *ACS Nano*, 6 (2012) 9291.
22. Nair, P. R., & Alam, M. A. (2007). Design Considerations of Silicon Nanowire Biosensors. *Electron Devices, IEEE Transactions on*, 54(12), 3400-3408.